Structural Mosaicism on the Submicron Scale in the Plasma Membrane

Rudolf Simson,* Bing Yang,* Stephen E. Moore,§ Patrick Doherty,§ Frank S. Walsh,§ and Ken A. Jacobson*#
*Department of Cell Biology and Anatomy, and #Lineberger Comprehensive Cancer Center, University of North Carolina, Chapel Hill, North Carolina 27599 USA, and §Department of Experimental Pathology, United Medical and Dental School, Guy's Hospital, London Bridge, London SE19RT, England

ABSTRACT The lateral mobility of the neural cell adhesion molecule (NCAM) was examined using single particle tracking (SPT). Various isoforms of human NCAM, differing in their ectodomain, their membrane anchorage mode, or the size of their cytoplasmic domain, were expressed in National Institutes of Health 3T3 cells and C2C12 muscle cells. On a 6.6-s time scale, SPT measurements on both transmembrane and glycosylphosphatidylinositol (GPI) anchored isoforms of NCAM expressed in 3T3 cells could be classified into mobile (Brownian diffusion), slow diffusion, corralled diffusion, and immobile subpopulations. On a 90-s time scale, SPT studies in C2C12 cells revealed that 40–60% of transfected NCAM was mobile, whereas a smaller fraction (~10–30%) experienced much slower diffusion. In addition, a fraction of ~30% of both transfected GPI and transmembrane isoforms and endogenous NCAM isoforms in C2C12 cells experienced transient confinement for ~8 s within regions of ~300-nm diameter. Diffusion within both these and the slow diffusion regions was anomalous, consistent with movements through a dense field of obstacles, whereas diffusion outside these regions was normal. Thus the membrane appears as a mosaic containing regions that permit free diffusion as well as regions in which NCAM is transiently confined to small or more extended domains. These results, including a large, freely diffusing fraction, similar confinement of transmembrane and GPI isoforms, a significant slowly diffusing fraction, and relatively large interdomain distances, are at some variance with the membrane skeleton fence model (Kusumi and Sako, 1996). Possible revisions to the model that incorporate these data are discussed.

INTRODUCTION

Domain structure in membranes has been postulated for 20 years or more (Jain and White, 1977), and large domains are well known in differentiated cells such as epithelium and cells of the reproductive system. However, there is less evidence for lateral heterogenity in the undifferentiated cell surface, and that which exists derives mainly from interpretations of various fluorescence studies. The large range of values obtained from typical fluorescence recovery after photobleaching (FRAP) studies (see, for example, Jacobson et al., 1987) has been taken as evidence for lateral heterogenity; and the presence of domains has been inferred from the dependence of the FRAP mobile fraction on laser beam diameter in the specimen plane (Yechiel and Edidin, 1987; Edidin, 1996). More directly, micron-sized lipid enrichments have been imaged by fluorescence in red cell ghosts (Rodgers and Glaser, 1993). The application of single-particle tracking (SPT) and laser trapping to plasma membrane components allows submicron domains to be investigated (see Jacobson et al., 1995; Kusumi and Sako, 1996). SPT permits observation of the movements of single or very small groups of proteins on a distance scale of tens of nanometers and on a time scale of tens of milliseconds. Based on SPT measurements of a major CAM, E-cadherin (Kusumi et al., 1993), the transferrin receptor and α_2-macroglobulin (Sako and Kusumi, 1994), as well as elegant laser trap and SPT measurements on the transferrin receptor (Sako and Kusumi, 1995), Kusumi and co-workers have proposed the membrane skeleton fence (Kusumi and Sako, 1996) as a general restraint to the mobility of membrane proteins.

Using SPT, the goal of this work was to determine the lateral mobility of various isoforms of another prominent cell adhesion molecule, the neural cell adhesion molecule (NCAM). The NCAM family consists of nearly 30 isoforms of cell adhesion molecules, which arise from a single gene that is alternatively spliced during transcription (Doherty et al., 1989, 1990a,b, 1992a,b; Pollerberg et al., 1986; Walsh and Doherty, 1991). Major isoform differences result either from various forms of membrane anchorage, including a membrane-spanning peptide with different sized cytoplasmic domains or a glycosylphosphatidyl-inositol (GPI) linkage. Cell type-specific ectodomain differences include a 37-amino acid insert, called the muscle-specific domain (MSD) (Walsh and Doherty, 1991), and a 10-amino acid insert derived from the VASE exon (Small et al., 1988; Doherty et al., 1992a). In addition to its role in cell adhesion, NCAM is involved in regulating neurite outgrowth (Doherty et al., 1989, 1990a,b, 1992a,b). The GPI-linked 120-kDa isoform and the 140-kDa isoform of NCAM, which contains a small cytoplasmic domain, are much more effective at promoting neurite outgrowth than the 180-kDa large cytoplasmic domain isoform (Doherty et al., 1992b).

Received for publication 25 March 1997 and in final form 22 September 1997.

Address reprint requests to Dr. Ken Jacobson, Department of Cell Biology and Anatomy, CB 7090, 108 Taylor Hall, University of North Carolina at Chapel Hill, Chapel Hill, NC 27599-7090. Tel.: 919-966-3855 or 919-966-5703; Fax: 919-966-1856; E-mail: frap@med.unc.edu.

Dr. Simson's present address is Department für Biophysik E22, Technische Universität München, München, Germany.

0006-3495/98/01/297/12 $2.00

The classification and analysis of NCAM SPT data revealed, in addition to free diffusion, the widespread existence of both corralled and very slow diffusing fractions for all isoforms. NCAM in these zones experienced a type of diffusion that can be interpreted as being strongly hindered by dense obstacle fields. These measurements indicate that the membrane is a mosaic containing regions that permit free diffusion as well as regions in which NCAM is confined for a range of times. Our measurements can be contrasted to those for E-cadherin (Kusumi et al., 1993). Such a comparison reveals significant differences between the lateral mobility of these two CAMs and indicates that either the membrane skeleton fence (Kusumi and Sako, 1996) is not a general restraint for all plasma membrane proteins, or that the way in which it restricts mobility depends on the particular protein.

MATERIALS AND METHODS

Cells and reagents

C2C12 mouse muscle cells and National Institutes of Health 3T3 fibroblasts were transfected with various isoforms of human NCAM as described elsewhere (Doherty et al., 1989; Peck and Walsh, 1993). Cells were routinely cultured in DMEM-H (Dulbecco's modified Eagle's medium, with D-glucose, L-glutamine, and sodium bicarbonate; H is for high glucose (9 g/liter)), supplemented with 10% fetal bovine serum, and plated on 22 mm × 22 mm coverslips for the SPT measurements 2 days before experiments. The anti-human NCAM (ERIC-1) is a mouse monoclonal antibody (mAb) IgG1 (Bourne et al., 1991); it was obtained from an ascites (Vector Labs, Burlingame, CA) and purified by ammonium sulfate precipitation, followed by a protein G column using the mAb Trap G11 Kit (Pharmacia). To label endogenous NCAM on C2C12 cells, anti-NCAM mAb H28 was employed (Gennarini et al., 1986). Fourty nanometer gold particles were conjugated to the antibody as previously described (Lee et al., 1991).

SPT measurements

SPT studies were performed essentially as described by Lee et al. (1991). Plated cells were incubated for 20 min with gold-conjugated antibody at 37°C in a CO_2 incubator and were examined on a Zeiss Axiovert 10 microscope with bright-field optics (100×, 1.3 NA oil-immersion objective and a 1.4 NA oil-immersion condenser). Cells were used for less than 1 h after labeling, and usually no evidence for internalization of gold-labeled antibody was found during this period, as judged by the fact that with bright-field optics, internalized gold probes are lower in contrast than gold probes on the cell surface.

Images were projected with a 4× adapter onto a Hamamatsu C2400 video camera and recorded on a Panasonic TQ-2028F optical disc recorder after real-time background subtraction and contrast enhancement, using Image 1 (Universal Imaging Corp., West Chester, PA). The data were analyzed by Image 1 to obtain the centroids of gold particles in each recorded frame, using a threshold function or cross-correlation analysis. Thresholding the diffraction pattern of gold tags yielded a pixel-size spatial resolution (~48 nm at the magnification used). Centroids could be localized to an accuracy of 20–30 nm by using a cross-correlation analysis as described by Gelles et al. (1988). The mean squared displacement (MSD) was calculated for every time interval previously described (Gross and Webb, 1988; Lee et al., 1991; Quian et al., 1991). Two-dimensional Brownian motion exhibits a linear relationship between the MSD and time ($\langle r^2 \rangle = 4Dt$), yielding a straight line of slope $4D$ in a plot of MSD versus time; regression analysis was used to obtain D from the initial slope of this plot.

Classification of short-term trajectories

The movements of the GPI-anchored NCAM120 and the transmembrane NCAM180 were examined in National Institutes of Health 3T3 fibroblasts over durations of 6.6 s (called short-term observations). Data sets consisting of 200 frames were recorded at video rate (33 ms/frame). Trajectories of NCAM observed on this time scale exhibited several distinct behaviors. Because just one mobility parameter would not have sufficed in separating different diffusional modes, we classified the data based on a combination of parameters. Trajectories could be separated into various classes based on D, the shape of the MSD-versus-time plot, and certain characteristics derived from the radius of gyration tensor (Saxton, 1993). The criteria that defined a given mobility class were chosen in a way that made it possible to assign each trajectory to one of the classes with little overlap. The selection of particular criteria was checked by comparision to simulated data (see below).

The shape of the MSD-versus-time plot allows different lateral transport modes to be distinguished. For example, if diffusion is confined to a corral of radius a, the MSD approaches a limiting value of a^2, reflecting the size of the corral. Following work by Saxton (1993), parameters derived from the radius of gyration tensor T (Eq. 1) were employed to characterize the shape, size, and asymmetry of trajectories:

$$T = \begin{pmatrix} \langle x^2 \rangle - \langle x \rangle^2 & \langle xy \rangle - \langle x \rangle \langle y \rangle \\ \langle xy \rangle - \langle x \rangle \langle y \rangle & \langle y^2 \rangle - \langle y \rangle^2 \end{pmatrix} \quad (1)$$

Here x and y are the coordinates of points that make up a trajectory, and the brackets denote an averaging over all points in the trajectory. The eigenvalues of T determine the major (R_1) and minor (R_2) semiaxes of an ellipse that approximates the size and shape of a trajectory. A standardized measure for the size of the trajectory is therefore provided by the squared radius of gyration, $Rg^2 = R_1^2 + R_2^2$. In the case of confined diffusion, Rg^2 also provides a measure for the size of the corral with $\langle r^2(t \to \infty) \rangle = 2Rg^2$ (Saxton, 1993). Two other parameters, $a_2 = R_2^2/R_1^2$ and $A_2 = (R_1^2 - R_2^2)/(R_1^2 + R_2^2)$, allow characterization of the asymmetry of the trajectory (Saxton, 1993). Although a_2 and A_2 are trivially related for a single trajectory, when averaged over a large set of tracks, they emphasize different parts of the asymmetry distribution. For a perfectly symmetrical trajectory, T describes a circle with $R_1 = R_2$, yielding $a_2 = 1$ and $A_2 = 0$. For a more asymmetrical trajectory, $R_1 > R_2$, and therefore $0 \leq a_2, A_2 < 1$. In the extreme asymmetrical case of the trajectory being a straight line, $R_1 = \infty$ and $R_1 = 0$, and therefore $a_2 = 0$ and $A_2 = 1$.

Short-term trajectories were divided into four classes, based on the following characteristics. The *mobile* class was defined by a linear MSD-versus-time curve, with $D > 1 \times 10^{-10}$ cm^2/s, $Rg^2 > 0.07$ μm^2, and $a_2 < 0.5$. The MSD-versus-time plot of the *slowly diffusing* class was approximately linear, but with $D < 1 \times 10^{-10}$ cm^2/s, $Rg^2 < 0.07$ μm^2, and $a_2 < 0.5$. The *corralled* class had a MSD-versus-time curve that approached a limiting value, $Rg^2 < 0.07$ μm^2 and $a_2 > 0.5$. The *immobile* class also exhibited a MSD-versus-time curve that plateaued, but with $D < 0.1 \times 10^{-10}$ cm^2/s and $Rg^2 < 0.015$ μm^2 with $a_2 > 0.5$. These criteria reflect the fact that the area covered by the trajectory within a certain time period, as characterized by Rg^2, will be greater for rapidly diffusing particles than for those with low diffusivity. Furthermore, immobilized or corralled diffusants usually produce more symmetrical trajectories that yield higher values for a_2, when compared to freely diffusing particles. Less than 3% of all trajectories did not fit perfectly into one of these categories. These trajectories were assigned to the class that best accounted for their characteristic parameters as defined above. In all cases, D was calculated from the initial slope of the MSD-versus-time plot.

Long-term trajectories and their classification

The diffusion of gold-labeled NCAM in C2C12 mouse muscle cells was examined on a longer time scale of 90 s, over which sets of 300 frames were recorded, at a frequency of one frame every 300 ms. A rigorous separation of trajectories into different classes as accomplished on the

shorter time scale was not possible, because a significant fraction of NCAMs switched between confined and free diffusion modes during the observation time. Because random diffusion can account for a wide variety of trajectory shapes and may temporarily mimic confinement (Berg, 1983), a comparison with simulated Brownian motion is necessary to determine if these apparent switches in diffusion mode cannot be accounted for by the large family of random walks. Accordingly, we developed a method for detecting temporary confinement that is not due to random diffusive behavior (Simson et al., 1995). Briefly, the probability ψ of small segments of a trajectory arising from Brownian motion is calculated according to the method of Saxton (1993):

$$\log(\Psi) = 0.2048 - 2.5117\, Dt/R^2 \qquad (2)$$

where R is the radius of a circle circumscribing the area covered by a segment of a trajectory during the time period t, and D is the diffusion coefficient. These probabilities are compiled to form a probability profile of that trajectory, in which regions exceeding a threshold level, L_c, denote periods of confinement due to nonrandom origins. The particular value of L_c chosen (3.16) corresponds to a probability of less than 1×10^{-4} that the underlying NCAM behavior arises from Brownian motion. Key parameters, including L_c, the segment size, and confinement time, have been optimized to minimize the detection of transient confinement in simulated random walks (Simson et al., 1995). For trajectories exhibiting more than one confinement event, the interconfinement zone distance was measured as the separation of the centers of successively visited confinement zones.

Trajectories switching between confined and free diffusion were combined in a new class termed *hybrid*. Furthermore, when observed at this longer time scale, practically no particle proved to be immobile according to the definition used for the short-term observations. All trajectories characterized by a value of $D < 0.1 \times 10^{-10}$ cm^2/s were therefore combined in a *slow* class. The remaining unconfined and rapidly diffusing proteins were again classified as *mobile*.

Detection of anomalous diffusion

NCAM trajectories have also been analyzed to determine whether diffusion is normal or anomalous. Motion through a dense field of obstacles can cause diffusion to be anomalous, in which case the MSD is no longer linear in time, but it is proportional to a power of time of less than 1, $\langle r^2 \rangle \propto t^{2/d_w}$, where d_w is the anomalous diffusion exponent. A plot of log(MSD/time) versus log(time) for normal diffusion yields a straight line of slope 0, whereas anomalous diffusion results in an initially negative slope given by $2/d_w - 1$ (Saxton, 1994). Anomalous diffusion is therefore characterized by a value of $d_w > 2$, whereas normal diffusion yields $d_w = 2$. For obstacle concentrations below the so-called percolation threshold, a cross-over to normal diffusion can be observed after a cross-over time t_c. Above this threshold, however, no long-range diffusion is possible, so no cross-over to normal diffusion can be observed (Saxton, 1994).

RESULTS

Lateral mobility of NCAM isoforms expressed in 3T3 cells

On a time scale of 6.6 s, both the GPI-anchored 120-kDa and the transmembrane 180-kDa isoforms of NCAM expressed in 3T3 cells exhibited four distinctly different subpopulations when examined by SPT, and were classified according to the criteria presented in Materials andMethods. Differences between characteristic trajectories of the four classes (mobile, slow, corralled, and immobile) can be seen in Fig. 1 and can be readily identified in a plot of the MSD versus time for each class (Fig. 2). Roughly 50% of the population for both isoforms exhibited rapid Brownian diffusion (the straight line of highest slope in Fig. 2). This fraction, called *mobile*, was characterized by a mean diffusion coefficient of 3.7×10^{-10} cm^2/s, about four- to sixfold lower than that measured by FRAP (Jacobson et al., 1997). Smaller fractions underwent *corralled* diffusion (the MSD approaching a limiting value with increasing time) or *slow* diffusion, or were classified as *immobile*. The average diffusion coefficients for each class were taken from the initial slope of their MSD curves in Fig. 2 and are listed in Table 1.

The quantities a_2 and A_2, although not independent, are both measures of the asymmetry of the trajectory, emphasizing different parts of the distribution. Simulations of unobstructed random walks yield, on average, $\langle a_2 \rangle = 0.28$ and $\langle A_2 \rangle = 0.39$ (Saxton, 1993), reflecting the fact that Brownian motion typically produces asymmetrical trajectories (Berg, 1983). NCAM classified as *mobile* come closest to these values (Table 1), consistent with the presumed Brownian nature of NCAM diffusion in this class. Proteins classified as *slow*, *corralled*, or *immobile*, however, yield different values for a_2 and A_2, reflecting a deviation from Brownian motion (Table 1). Trajectories in the classes *corralled* or *immobile* are more symmetrical, yielding higher values for a_2, whereas trajectories in the *slow* category are more asymmetrical as compared to trajectories for Brownian motion. Differences in the values for Rg^2 reflect the fact that trajectories from rapid diffusing proteins cover a larger membrane area within a certain time period than slowly diffusing proteins (Table 1). For *corralled* NCAM, however, exhibiting a diffusivity comparable to that of NCAM in the class *mobile*, Rg^2 simply corresponds to an average corral diameter of ~300 nm.

The classification scheme was checked for self-consistency for the *mobile* and *slow* classes by simulating random walks characterized by the experimentally obtained D values for NCAM 120 and 180, respectively, and then calculating the fraction of trajectories that would be misclassified as corralled according to our criteria (Table 2). These simulations show that the probability of wrongly classifying a trajectory as corralled increases as the D value decreases. For example, for the fastest diffusing class, *mobile,* only ~3% of the simulated trajectories would have been classsified as corralled. In the case of the slow class, the trajectories failing to match the condition in a_2 for slow Brownian diffusion would necessarily satisfy the condition for corralled because the criteria for slow and corralled differ only in a_2. In this case 11.5% of the trajectories would have been misclassifed as corralled. On the other hand, if we simulate Brownian diffusion for the range of D values obtained for the corralled diffusion of NCAM 120 and 180, only 8.4% and 5.6%, respectively, would have qualified as corralled (last two rows of Table 2). As discussed in Materials and Methods, movements through a dense field of obstacles can cause diffusion to become anomalous; this phenomenon yields an initially negative slope in a plot of log(MSD/time) versus log(time) and an anomalous diffusion exponent $d_w > 2$. On the same plot, normal diffusion yields a straight line

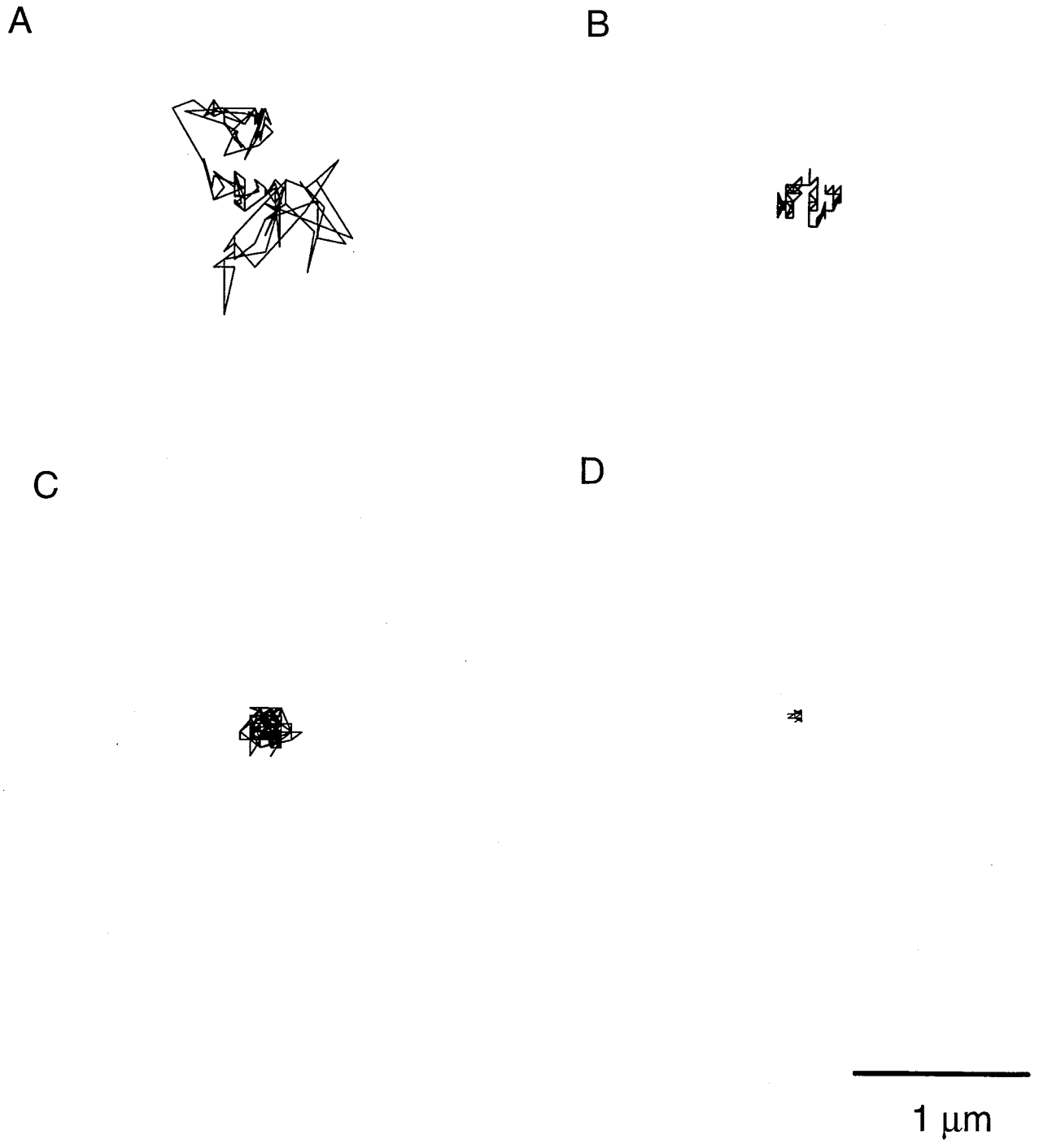

FIGURE 1 Representative trajectories of the various classes (NCAM 180 transfected into 3T3 cells) of short-term (6.6 s) measurements. (*A*) Mobile; (*B*) slow; (*C*) corralled; (*D*) immobile.

of slope 0, or $d_w = 2$. We applied this test to both NCAM180 and NCAM120 for the 6.6-s observation times. Linear regression yields an initial slope of ~ -0.07, or $d_w \approx 2.1$, for the *mobile* fractions of both isoforms (Fig. 3 *a*), indicating that diffusion is indeed normal for NCAM in this class. For the classes *slow* and *corralled*, however (Fig. 3, *b* and *c*, respectively), the results suggest that diffusion is anomalous, with anomalous diffusion exponents between $d_w \approx 4$ and $d_w \approx 7$ (Table 3).

Lateral mobility of NCAM isoforms expressed in C2C12 muscle cells

The behavior of transfected isoforms (NCAM125, NCAM140) and endogenous isoforms (predominantly NCAM140) was examined in muscle cells on the longer time scale of 90 s; endogenous NCAM was also investigated on the short-term time scale (Table 1). The predominant NCAM expressed in the myoblast stage is the trans-

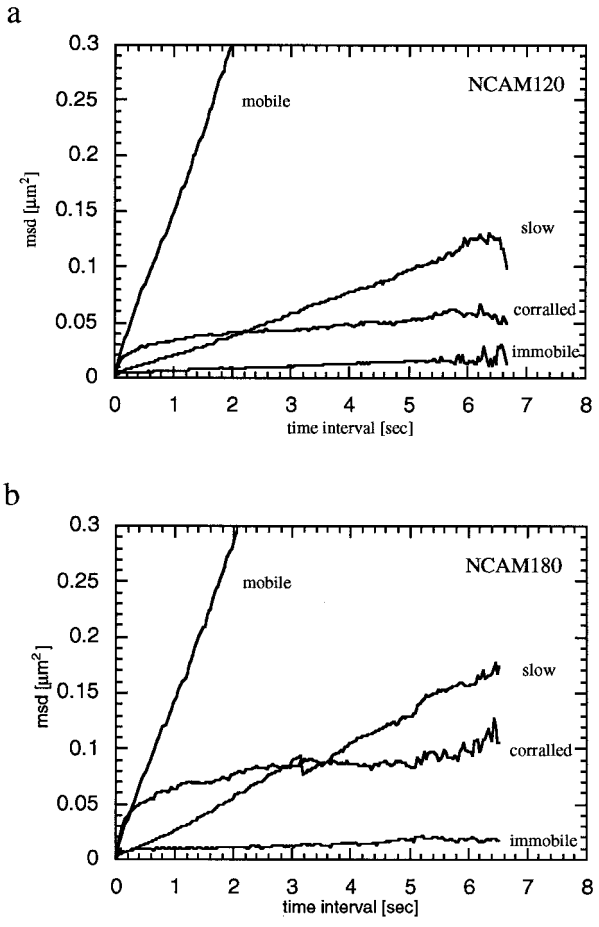

FIGURE 2 Different modes of diffusion (classes) detected in a plot of mean squared displacement (MSD) versus time interval for NCAM120 (*a*) and NCAM180 (*b*). The fastest diffusing class (mobile) is characterized by the steepest slope. The MSD for the corralled fractions approaches a limiting value with increasing time, which is a measure of corral size.

membrane 140-kDa isoform, whereas the 125-kDa isoform is more prevalent in myotubes (Moore et al., 1987). Although NCAM125 is a GPI-anchored protein and NCAM140 is a transmembrane protein, all isoforms showed roughly similar behavior in the long-term observations. The mobile class for the endogenous NCAM140 was characterized by a lateral diffusion coefficient somewhat greater than that for the two transfected isoforms (Table 4). Furthermore, endogeneous NCAM showed appreciably more corralled diffusion in the long term (hybrid, Table 4) and in the short term (Table 1) than did the isoforms expressed by gene transfer.

A considerable fraction (15–40%) of all isoforms exhibited free Brownian diffusion interspersed with periods of transient confinement, and are referred to as the *hybrid* class. Periods of transient confinement were identified by probability profile analysis (Simson et al., 1995) (Fig. 4); they have a likelihood of less than 1×10^{-4} of arising from Brownian motion. By the same analysis, confined periods were detected in only 1.5% of 1100 simulated random walks (Table 5; Simson et al., 1995). The range of confinement times, confinement zone radii, and interconfinement zone separations is given by the histograms in Fig. 5 for NCAM 125 (Fig. 5, *a–c*) and endogenous NCAM (Fig. 5, *d–f*). NCAM in the hybrid class typically exhibited one or two confined periods, each lasting ~7 s and occurring within a region with a diameter of ~300–400 nm (Table 4). The interconfinement zone separations were distributed over a range of distances from less than 0.5 μm to over 2 μm. A large fraction, ~50%, had only one confinement zone per trajectory, which suggests a large separation of successive confinement zones.

The remaining fraction of the NCAM could be separated into a *mobile* class, exhibiting unconfined Brownian diffusion, and a *slowly* diffusing class, that contained proteins with D values less than 0.1×10^{-10} cm^2/s (Table 5). Although they diffused very slowly, these proteins were not immobile by the standards set for the 6.6-s studies.

Tests for anomalous diffusion were also conducted for NCAM diffusion in muscle cells. For all three isoforms, NCAM125, NCAM140, and the endogenous NCAM140, the log-log plot for the unconfined diffusing proteins in the *mobile* class yields values of d_w between 1.9 and 2.2, indicating that diffusion is normal (Table 3). NCAMs in the *slow* class exhibit anomalous diffusion, with d_w between 3 and 4 (Table 3). The same analysis for only the confined parts of the *hybrid* trajectories suggests that diffusion within the confinement zones is anomalous, with $d_w \geq 6$ for all NCAM isoforms (Table 6, "corralled"), whereas diffusion appears normal during the unconfined periods (data not shown).

DISCUSSION

SPT results demonstrate the existence of transient confinement and slow diffusion zones

These SPT results expand our understanding of membrane protein mobility by increasing both the time and spatial resolution of the mobility determination. They indicate that a significant fraction of NCAM exhibits confined, hindered diffusion. Short-term SPT results could be classified into mobile (Brownian) diffusion, corralled diffusion, slow diffusion, and immobile fractions. On this time scale, proteins maintained a single diffusion mode during the entire period of observation. Notably, only ~50% of the labeled population exhibited normal, Brownian diffusion. Neither the D value for the mobile class nor the distribution of trajectories into the various classes depended significantly on the mode of membrane anchorage (GPI anchorage for NCAM 120 versus membrane-spanning peptide with large cytoplasmic domain for NCAM 180). The similarity of SPT-derived D values for the mobile classes of NCAM 120 and 180 in particular is consistent with earlier FRAP results on vesicular stomatitis G glycoprotein membrane anchorage mutants (Zhang et al., 1991) and various NCAM isoforms with different membrane anchors (Jacobson et al., 1997). In these cases, the D value characterizing the mobile fraction showed little dependence on the mode of membrane anchorage when mutants or isoforms with similar or identical ectodomains were compared. To examine whether proteins

TABLE 1 Average values (± SE) for parameters characterizing each class of 6.6-s trajectory for human NCAM120 and NCAM180 in 3T3 fibroblasts and endogenous NCAM 140 in C2C12 muscle cells

	Fraction (%)	D (10^{-10} cm^2/s)	a_2	A_2	R_g^2 (μm^2)
NCAM120-3T3 (n = 191)					
Mobile	52	3.7 ± 0.14	0.25 ± 0.003	0.44 ± 0.008	0.164 ± 0.0003
Slow	16	0.6 ± 0.08	0.18 ± 0.004	0.51 ± 0.001	0.022 ± 0.0001
Corralled	22	1.8 ± 0.28	0.49 ± 0.006	0.15 ± 0.003	0.019 ± 0.0002
Immobile	10	0.06 ± 0.01	0.46 ± 0.0003	0.20 ± 0.009	0.005 ± 4.6e-5
NCAM180-3T3 (n = 191)					
Mobile	50	3.7 ± 0.18	0.24 ± 0.003	0.46 ± 0.007	0.153 ± 0.002
Slow	14	0.5 ± 0.09	0.13 ± 0.003	0.64 ± 0.01	0.028 ± 7.3e-5
Corralled	21	3.4 ± 0.33	0.48 ± 0.008	0.19 ± 0.006	0.036 ± 0.0001
Immobile	15	0.04 ± 0.02	0.50 ± 1.8e-5	0.15 ± 0.004	0.006 ± 2.5e-5
Endogenous NCAM140-C2C12 (n = 101)					
Mobile	15	4.5 ± 0.61	0.25 ± 0.03	0.40 ± 0.05	0.109 ± 0.016
Slow	30	0.5 ± 0.06	0.23 ± 0.02	0.43 ± 0.04	0.012 ± 0.002
Corralled	49	1.9 ± 0.27	0.58 ± 0.02	0.08 ± 0.01	0.020 ± 0.003
Immobile	6	0.07 ± 0.01	0.50 ± 0.09	0.16 ± 0.05	0.001 ± 0.0001

The numbers of trajectories examined for each isoform are given in parentheses.

within corrals can ever leave them, two transfected NCAM isoforms, NCAM125 and NCAM140, and an endogenous isoform, NCAM140, were examined on a much longer time scale of 90 s in C2C12 muscle cells. Roughly 20–40% of the populations of both the transfected GPI-anchored 125 kDa and the transmembrane 140-kDa isoforms as well as the endogenous NCAM isoforms exhibited hybrid trajectories in which the particle switched between unrestricted Brownian and confined diffusion. Although the size of the confinement zones and duration of confinement may vary, this behavior is not unique to NCAM (for a review, see Sheets et al., 1995). The remaining NCAM exhibited either rapid Brownian or slow, anomalous diffusion.

NCAM diffusion within transient confinement zones and slow diffusion zones is anomalous

Within confinement zones, diffusion was anomalous for both the GPI and transmembrane NCAM isoforms expressed in muscle and 3T3 cells. These results suggest that a high concentration of obstacles exists within the confinement zones. A dense field of obstacles on the cell surface could entrap both transmembrane and lipid-linked proteins like the ball in a pinball machine. However, diffusion was normal for the *mobile* NCAM, both in fibroblasts and in muscle cells. These results indicate that some regions of the plasma membrane exhibit diffusion unhindered by obstacles, reflecting a marked heterogeneity of the membrane structure.

Models for slow diffusion and transient confinement zones

A way to think about the NCAM results is to assume that both TCZs and slow diffusion regions are both obstacle-rich regions, but of different sizes. In the smaller TCZs, the particle is confined, but only temporarily, whereas in the larger slow diffusion regions, the particle experiences con-

TABLE 2 Misclassification of simulated random walks

Category	Mean value of D used for simulating Brownian diffusion*	Fraction of simulated trajectories wrongly classified as corralled#
Mobile (Brownian)		
Mean $D = 3.7 \times 10^{-10}$ cm^2/s	3.7×10^{-10} cm^2/s	3%
$R_g^2 > 0.07$ μm^2; $a_2 < 0.5$		
Slow		
Mean $D = 0.5 \times 10^{-10}$ cm^2/s	0.5×10^{-10} cm^2/s	11.5%
$R_g^2 < 0.07$ μm^2; $a_2 < 0.5$		
Corralled NCAM120		
Mean $D = 1.8 \times 10^{-10}$ cm^2/s	1.8×10^{-10} cm^2/s	8.4%
$R_g^2 < 0.07$ μm^2; $a_2 > 0.5$		
Corralled NCAM180		
Mean $D = 3.4 \times 10^{-10}$ cm^2/s	3.4×10^{-10} cm^2/s	5.6%
$R_g^2 < 0.07$ μm^2; $a_2 > 0.5$		

*Mean D value of a distribution employed for simulating 30,000 Brownian trajectories. It matches the experimental mean D value for the respective class. For the NCAM 180 and 120 isoforms, the D values for the mobile and slow classes were almost identical (Table 1).

#Fraction of simulated trajectories that meet the criteria for corralled diffusion ($R_g^2 < 0.07$ μm^2; $a_2 > 0.5$), despite their Brownian nature.

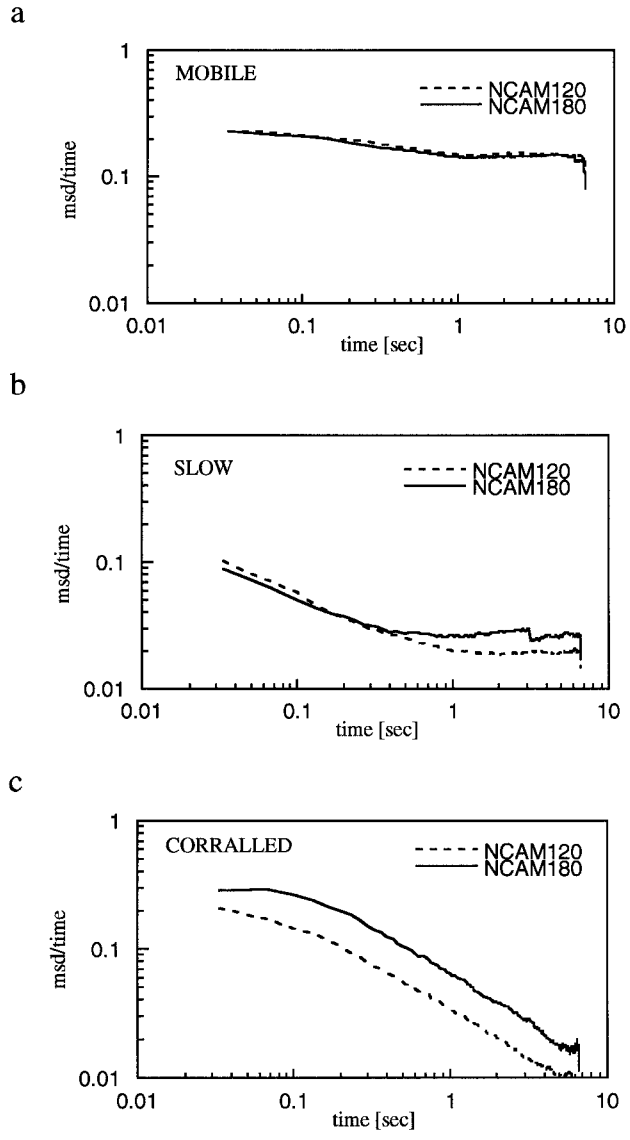

FIGURE 3 Tests for anomalous diffusion for mobile (*a*), slow (*b*), and corralled (*c*) classes for both NCAM 120 and 180 expressed in 3T3 cells. Fitting parameters are given in Table 3.

TABLE 3 Value of anomalous diffusion exponent for various NCAM populations*

	Class	Initial slope	Goodness of fit (R^2)	d_w
3T3 cells				
NCAM120#	Mobile	−0.06	0.93	2.13
	Slow	−0.57	0.99	4.65
	Corralled	−0.69	0.99	6.45
NCAM180#	Mobile	−0.08	0.99	2.17
	Slow	−0.49	0.99	3.92
	Corralled	−0.71	0.98	6.89
C2C12 cells				
NCAM125#	Mobile	−0.08	0.6	2.17
	Slow	−0.53	0.99	4.26
	Corralled	−0.86	0.99	14.3
NCAM140#	Mobile	−0.02	0.4	2.04
	Slow	−0.44	0.99	3.57
	Corralled	−0.66	0.96	5.88
NCAM140§	Mobile	0.07	0.6	1.87
	Slow	−0.33	0.99	2.98
	Corralled	−0.74	0.96	7.69

*Detection of a negative initial slope of $2/d_w - 1$ in a plot of log(MSD/time) versus log(time) indicates anomalous diffusion, with an anomalous diffusion exponent d_w. Normal diffusion yields slope 0 or $d_w = 2$.
#Human NCAM isoform expressed by transfection.
§Endogenous isoform.

strained, anomalous diffusion for the entire period of observation.

What molecular structures might give rise to this constrained diffusion? Current concepts for the restraints to lateral mobility have been reviewed recently (Sheetz, 1993; Zhang et al., 1993; Edidin, 1996; Saxton and Jacobson, 1997). These range from the membrane skeleton fence model (Kusumi and Sako, 1996; see below) to lipid lateral domain structure (see, for example, Sheets et al., 1995), to a generalized system of fluctuating barriers with no fixed time or length scale (Feder et al., 1996). The latter concept includes the possibility of transient associations between the diffusant and other membrane components, and such associations could occur in the extracellular, bilayer, or cytoplasmic regions. One noteworthy result is that confinement parameters (percentage confined in the short-term data and the size and duration of the confinment zones from the long-term data) were similar for both transmembrane and GPI-anchored isoforms; this suggests that one mechanism could apply to both forms of membrane anchorage.

Confinement based on the membrane-apposed cytoskeleton

Anomalous diffusion could arise from proteins tethered to the membrane skeleton (Fig. 6 *a*). Such a scheme could account for the transient confinement and slow diffusion of both transmembrane and GPI-anchored proteins; it is attractive because the average domain size and duration of confinement are similar for both isoforms. Alternatively, the skeleton itself could constitute the obstacle field, as the elementary corral size (Peters, 1988), based on the red cell model, is often much smaller than the confinment zone diameters that are measured.

Confinement based on lipid domains

Although the obstacles causing anomalous diffusion could be proteins directly or indirectly linked to the membrane skeleton as described above, another possible mechanism of confinement of GPI-linked proteins is regional differences in the lipid composition of the membrane bilayer (Fig. 6 *b*). Many GPI-anchored proteins co-isolate with a detergent-inextractable fraction enriched in glycolipids and cholesterol (Brown and Rose, 1992). Such fractions can be isolated from lung tissue as vesicles, and their diameter measured by transmission electron microscopy (Schnitzer et

TABLE 4 Average values (± SE) for parameters characterizing each class of 90-s trajectory for human NCAM125 and NCAM140 and endogenous NCAM (NCAM140) in C2C12 muscle cells in the myoblast stage

	Fraction (%)	D (10^{-10} cm^2/s)	a_2	A_2	R_g^2 (μm^2)
NCAM125 (n = 112)					
Mobile	39	0.89 ± 0.18	0.26 ± 0.03	0.42 ± 0.04	0.41 ± 0.07
Hybrid	28	1.33 ± 0.19	0.18 ± 0.03	0.54 ± 0.05	0.78 ± 0.14
Slow	33	0.04 ± 0.005	0.29 ± 0.04	0.41 ± 0.04	0.02 ± 0.004
NCAM140 (n = 96)					
Mobile	64	1.12 ± 0.14	0.27 ± 0.02	0.42 ± 0.03	0.60 ± 0.09
Hybrid	14	1.43 ± 0.46	0.27 ± 0.05	0.42 ± 0.06	0.67 ± 0.18
Slow	22	0.06 ± 0.01	0.37 ± 0.04	0.26 ± 0.03	0.03 ± 0.005
Endogenous NCAM140 (n = 51)					
Mobile	53	3.47 ± 0.54	0.20 ± 0.03	0.51 ± 0.04	2.05 ± 0.34
Hybrid	37	3.31 ± 0.38	0.34 ± 0.04	0.31 ± 0.05	1.58 ± 0.29
Slow	10	0.05 ± 0.02	0.45 ± 0.09	0.24 ± 0.13	0.08 ± 0.04

The numbers of trajectories examined for each isoform are given in parentheses.

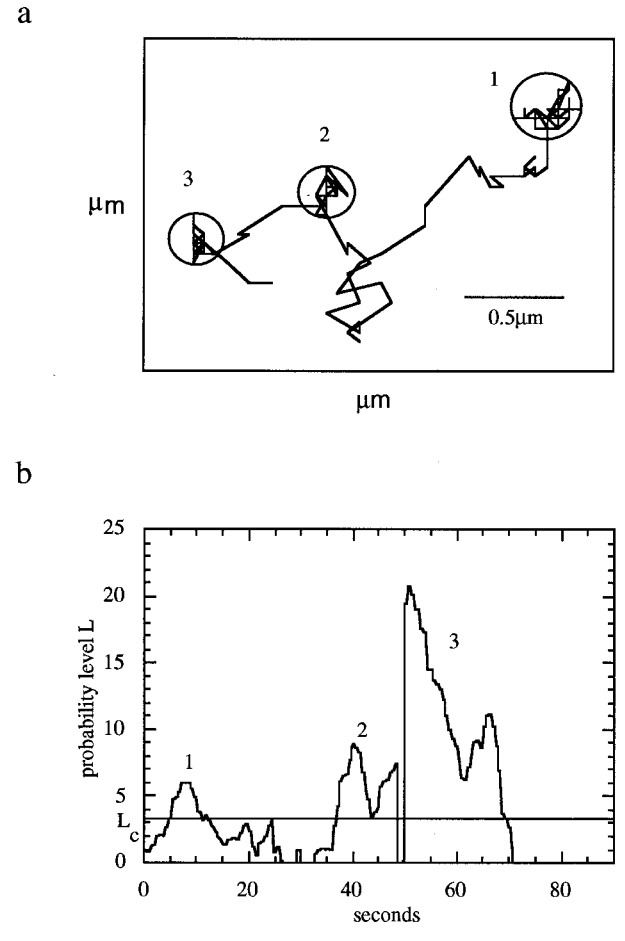

FIGURE 4 Trajectory and the corresponding probability profile are shown for a lipid linked NCAM125, observed for 90 s in C2C12 muscle cells. The probability level L is given as $-\log(\psi) - 1$, where ψ is the probability that the underlying NCAM behavior is Brownian. Transient confinement is defined to occur in regions of the profile (b) where L rises above a threshold level $L_c = 3.16$, corresponding to a probability of less than 1×10^{-4} that the NCAM behavior was Brownian. In this example, three periods of confinement were detected in the probability profile (b), corresponding to the circled and numbered regions in the trajectory (a). Note that confinement zone 3 has a probability of less than 1×10^{-22} of arising from Brownian motion, because peak 3 reaches a level $L \approx 21$ (b).

al., 1995). If such vesicles were discs on the plasma membrane, their diameters would be ~400 nm, close to what is measured for confinement zones by SPT. In this regard, it is interesting that the glycolipid GM_1 labeled with cholera toxin also shows transient confinement zones of a size similar to that of confinement zones seen for NCAM (Sheets et al., 1997). Assuming that glycolipid-enriched fractions are not artifacts of detergent isolation, the obstacles causing anomalous diffusion might be liquid ordered or gel-like microphases existing within each transient confinement zone (Schroeder et al., 1994).

Comparison of SPT results for NCAM and E-cadherin: general applicabilty of the membrane skeleton fence model

The membrane skeleton fence model (Kusumi and Sako, 1996) is a conceptually straightforward basis for transient confinement of diffusing proteins. This model is based on earlier work on the erythrocyte membrane (Golan and Veatch, 1980; Sheetz et al., 1980; Tsuji and Ohnishi, 1986). The fence structure consists of spectrin, actin, and ankyrin or their analogs, forming a meshwork apposed to the cytoplasmic leaflet. Confinement of transmembrane proteins

TABLE 5 Transient confinement detected in NCAM trajectories and simulated random walks

	Trajectories with conf. zones (%)	Diameter of conf. zones* ±SD (nm)	Duration of conf. zones* ± SD (s)
NCAM125[#]	27.7	280 ± 160	7.2 ± 4.5
NCAM140	13.5	224 ± 140	6.2 ± 4.4
NCAM140 (endogenous)	37.3	460 ± 280	6.5 ± 3.4
Simulated random walks[#]	1.5	270 ± 196	3.1 ± 0.2

*Results are averaged over trajectories that contained at least one confinement zone.

[#]Results are taken from Simson et al. (1995).

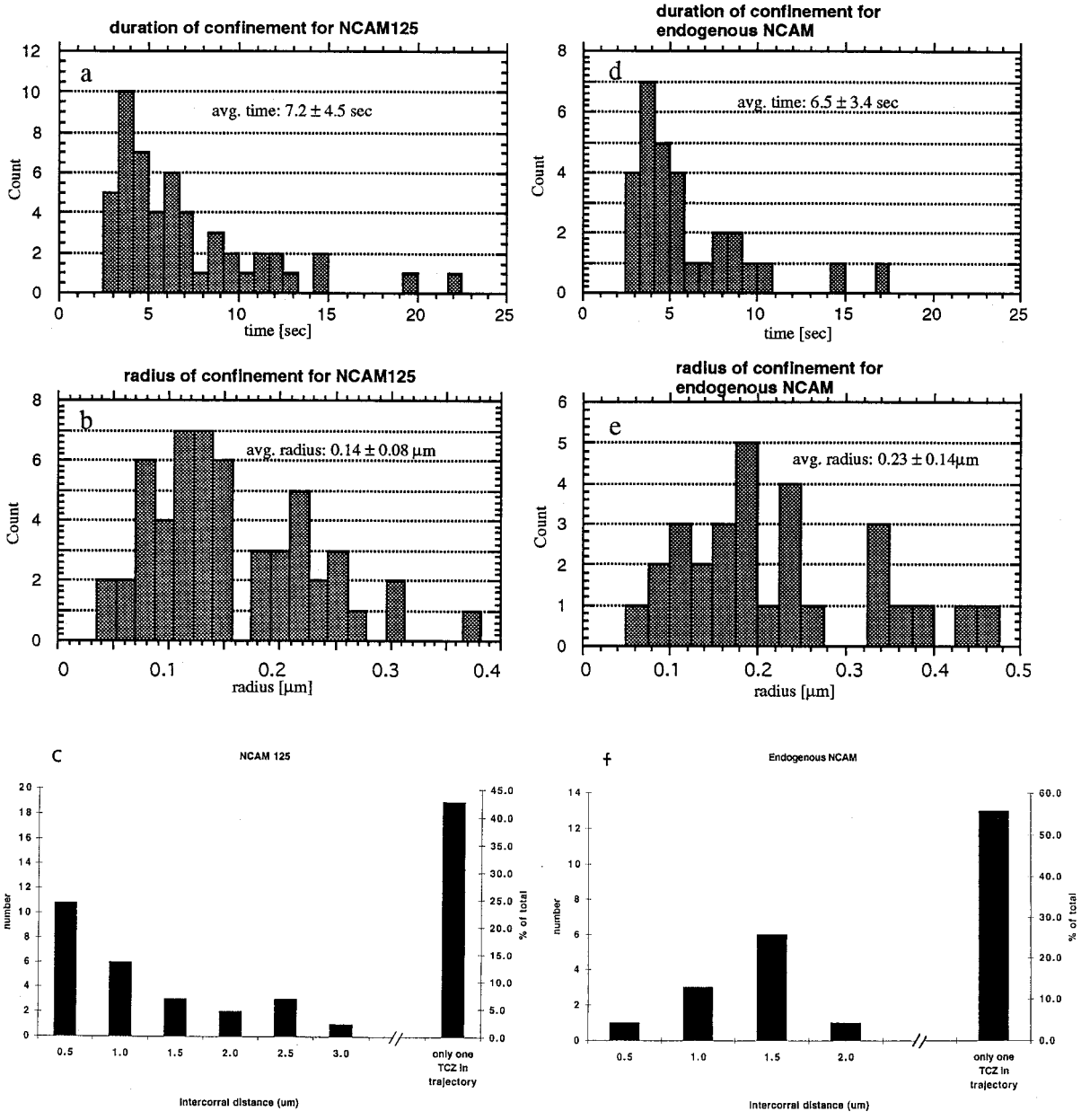

FIGURE 5 (*a, b, d, e*) Histograms of the distribution of confinement times and confinement zone radii. (*a*, *b*) Human NCAM 125 expressed in C2C12 muscle cells. (*d*, *e*) Endogenous NCAM (predominantly NCAM140) in C2C12 muscle cells. (*c*, *f*) Histograms of interconfinement zone separations. (*c*) Human NCAM 125 expressed in C2C12 cells; (*f*) endogenous NCAM (predominantly NCAM 140) in C2C12 muscle cells. In both histograms, the tallest bar to the right represents the fraction of trajectories with only one confinement zone detected.

occurs when their cytoplasmic domains are entrapped by this meshwork. Thermally induced fluctuations or dissociation of the cytoskeleton meshwork are proposed to account for the transient nature of the confinement by allowing movement of the membrane protein from one confinement zone to an adjacent one (Kusumi and Sako, 1996).

It is instructive to compare the mobility results for two members of two prominent CAM families: NCAM 140 and E-cadherin. Both are single spanning transmembrane proteins of similar molecular weight and cytoplasmic domain size: NCAM 140 has a cytoplasmic domain size of ~13 kDa versus ~16 kDa for E-cadherin. Some of the cytoplasmic domain binding partners for E-cadherin, the catenins, are known (Ranscht, 1994; Kemler, 1993).

Inspection of Table 6 reveals that the data for NCAM 140 do not fit the membrane skeleton fence model as nicely as do the results for E-cadherin (Kusumi et al., 1993). First, as measured by FRAP, the long-range lateral diffusion coefficient for NCAM 140 is nearly 30 times greater than that for E-cadherin. This large difference is presumbably due to the constraints the membrane skeleton fence confers on E-cadherin diffusion. SPT studies reveal that over half of NCAM undergoes rapid Brownian diffusion, whereas only 10% of the E-cadherin does. About one-third of both pro-

TABLE 6 Comparison of NCAM 140 and E-cadherin lateral mobility*

Biological system	NCAM 140 (endogenous NCAM expressed in C2C12 muscle cells)	E-cadherin (in cultured mouse keratinocytes; low Ca^{2+})
FRAP studies		
D (cm^2/s)	$6.9\ (\pm 0.2) \times 10^{-10}$[#]	2.6×10^{-11}
Mobile fraction (%)	51%[#]	75%
SPT studies		
Brownian diffusion	3.5×10^{-10} (53%)	3.2×10^{-11} (11%)
Fraction of confined diffusion and intra domain D (cm^2/s)	37%; [$3.3\ (\pm 0.4) \times 10^{-10}$]	30%; [$<1 \times 10^{-12}$ to $\sim 2 \times 10^{-10}$] ($\sim$67% in high Ca^{2+})
Residence time	mean: 6.5 ± 3.4 s[§]	3–30 s
Domain diameter	460 ± 280 nm[§]	300–600 nm
Intercorral distance	Broad distribution from <0.5 to >2.0 μm	0.3–0.6 μm[¶]
Fraction of stationary particles	0	22%
% directed	0	37%

*NCAM140 is the predominant endogenous isoform expressed in myoblasts. E-cadherin data are for keratinocytes in low Ca^{2+} (50 μM) where the cells remain morphologically undifferentiated.

[#]From Yang et al. (submitted); values ($\pm$ SEM).

[§]Values ($\pm$SD).

[¶]Based on the membrane skeleton fence model's postulate that E-cadherin jumps from one corral to the adjacent one, implying a mean intercorral distance of $\sim$450 nm.

teins are transiently confined, and roughly speaking, the confinement times and domain diameters are similar, although in high-Ca^{2+} medium fully two-thirds of E-cadherin is confined (Kusumi et al., 1993). But the interdomain distances are different: NCAM 140 interdomain separations are broadly distributed from <0.5 μm to over 2 μm, with the largest fraction of trajectories showing only one transient confinement zone (Fig. 5, *c* and *f*). In contrast, E-cadherin is thought to move from one confinement zone to the adjacent one, a distance of 300–600 nm (Kusumi et al., 1993). Last, there are no immobile NCAM on the 90-s time scale, but $\sim$20% of the E-cadherin is immobile; and no NCAM shows directed motion, but 37% of E-cadherin does.

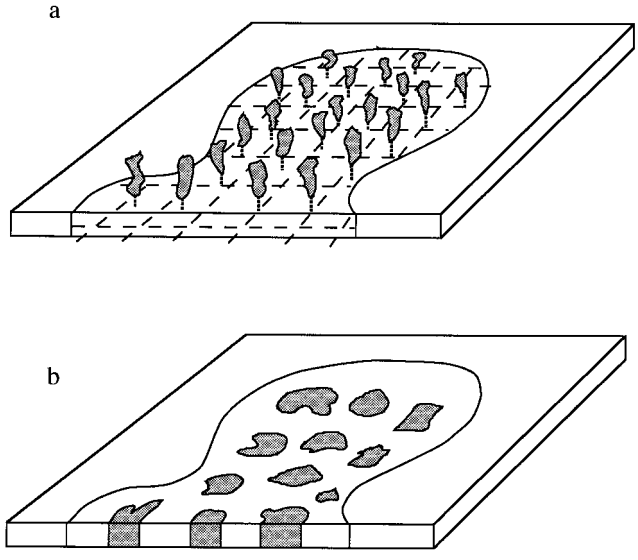

FIGURE 6 Models for confined diffusion zones. (*a*) Confinement-based membrane skeleton fence (Kusumi and Sako, 1996). In this version, anomalous diffusion is caused by protein obstacles tethered to the cytoskeleton and/or the cytoskeletal filaments themselves. (*b*) Confinement based on largely impenetrable lipid microdomains (*shaded regions*), which provide the obstacle field, giving rise to anomalous diffusion.

How can these discrepencies be interpreted? If we take the membrane skeleton fence model as providing the preferred length and time scales for confinement, some revision of the model is required to incorporate the NCAM data. It is important to note that this generalized restraint must be at least temporarily inoperative to permit half of the labeled NCAM 140 to diffuse normally and rapidly. This could mean that in certain regions of the plasma membrane, the skeleton-membrane distance is too great to constrain the mobility of some or all membrane proteins or, alternatively, that membrane regions exist that have no skeleton intimately associated with them. One reason that the skelton-membrane distance is too great to regulate mobility could be that the size of the NCAM domain may be too small to interact with the skeleton except occasionally, and as a result, the intercorral distance is greater for NCAM. Because E-cadherin can have its cytoplasmic domain further expanded by association with catenins, it may interact more continously with the skeleton, leading to its hopping from one domain to an adjacent one. Indeed, Kusumi and coworkers have shown by both SPT and laser trapping that mutants of E-cadherin truncated in their cytoplasmic domain have considerably larger confinement zones (Kusumi et al., personal communication). Such truncation may abolish the association with cytoplasmic molecules.

It is also possible that whereas proteins such as the cadherins are directly confined by the cytoskeletal network underlying the membrane, proteins with smaller cytoplasmic domains or GPI anchors are confined indirectly by interacting via their ecto- or membrane anchorage domains with other membrane proteins that are bound to the cytoskeleton (Sheets et al., 1995).

Gold particle effects on lateral diffusion

In general, diffusion coefficients measured by SPT for the highly mobile fraction of a given membrane component are a factor of 2 to 6 lower than those measured by FRAP for that membrane component without a particle attached (for a review, see Saxton and Jacobson, 1997). For NCAM, we have recorded similar differences in comparing the SPT and FRAP values (see Table 6). The size of the gold particle (40-nm diameter) and its potential to link to one or several NCAMs make it plausible that the *D* values measured for the mobile fractions by SPT would be smaller than those measured by FRAP. In general, the effect of these two factors on the measured mobility properties has not been completely resolved. However, work by Sheets et al. (1997) from this laboratory shows that the classification of trajectories as well as the size and duration of the transient confinement zones for particles attached to the membrane protein Thy 1 are independent of the apparent valency of the particle.

CONCLUSIONS

Although it is tempting to accept the membrane skeleton fence model as a plausible general extension of the red cell membrane structure to other mammalian cells, there are a number of features of the NCAM data that do not immediately fit into this paradigm. These include a large fraction of randomly diffusing particles, similar confinement of GPI-anchored and transmembrane proteins, and larger interdomain distances for NCAM compared to E-cadherin. Furthermore, that a significant fraction of particles diffuse slowly and anomalously is not directly accounted for by the membrane skeleton fence model. The strength of the model will ultimately be judged on its capability to accommodate such apparently discordant results.

The authors thank Erin Sheets, Michael Saxton, and Watt Webb for helpful discussions.

This work was supported by National Institutes of Health grant GM 41402 (KAJ) and the Muscular Dystrophy Group of Great Britain and the Wellcome Trust (FSW and PD).

REFERENCES

Berg, H. C. 1983. Random Walks in Biology. Princeton University Press, Princeton, NJ. 5–12.

Bourne, S. P., K. Patel, F. S. Walsh, C. T. Popham, H. B. Coakaam, and J. T. Kemshead. 1991. A monclonal antibody (ERIC-1) raised against retinoblastoma that recognises the neural cell adhesion molecule (NCAM) expressed on brain and tumours arising from the neuroectoderm. *J. Neurooncol.* 10:119.

Brown, D. A. 1992. Interactions between GPI-anchored proteins and membrane lipids. *Trends Cell Biol.* 2:338–343.

Brown, D. A., and J. K. Rose. 1992. Sorting of GPI-anchored proteins to glycolipid-enriched membrane subdomains during transport to the apical cell surface. *Cell.* 68:533–544.

deBrabander, M., R. Nuydens, A. Ishihara, B. Holifield, K. Jacobson, and H. Geerts. 1991. Lateral diffusion and retrograde movements of individual cell surface components on single motile cells observed with nanovid microscopy. *J. Cell Biol.* 112:111–124.

Doherty, P., C. H. Barton, G. Dickson, P. Seaton, L. H. Rowett, S. E. Moore, H. J. Gower, and F. S. Walsh. 1989. Neuronal process outgrowth of human sensory neurons on monolayers of cells transfected with cDNAs for five human NCAM isoforms. *J. Cell Biol.* 109:789–798.

Doherty, P., J. Cohen, and F. S. Walsh. 1990a. Neurite outgrowth in response to transfected NCAM changes during development and is modulated by polysialic acid. *Neuron.* 5:209–219.

Doherty, P., M. Fruns, P. Seaton, G. Dickson, C. H. Barton, T. A. Sears, and F. S. Walsh. 1990b. A threshold effect of the major isoforms of NCAM on neurite outgrowth. *Nature.* 343:464–466.

Doherty, P., C. E. C. K. Moolenaar, S. V. Ashton, R. J. A. M. Michalides, and F. S. Walsh. 1992a. The VASE exon downregulates the neurite growth-promoting activity of NCAM140. *Nature.* 356:791–793.

Doherty, P., G. Rimon, D. A. Mann, and F. S. Walsh. 1992b. Alternative splicing of the cytoplasmic domain of neural cell adhesion molecule alters its ability to act as a substrate for neurite outgrowth. *J. Neurochem.* 58:2338–2341.

Edidin, M. 1996. Getting there is only half the fun. *Curr. Top. Membr.* (in press).

Edidin, M., S. C. Kuo, and M. P. Sheetz. 1991. Lateral movements of membrane glycoproteins restricted by dynamic cytoplasmic barriers. *Science.* 254:1379–1382.

Edidin, M., M. C. Zúñiga, and M. P. Sheetz. 1994. Truncation mutants define and locate cytoplasmic barriers to lateral mobility of membrane glycoproteins. *Proc. Natl. Acad. Sci. USA.* 91:3378–3382.

Feder, T. J., I. Brust-Mascher, J. P. Slattery, B. Baird, and W. W. Webb. 1996. Constrained diffusion or immobile fraction on cell surfaces: a new interpretation. *Biophys. J.* 70:2767–2773.

Geerts, H., M. deBrabander, R. Nuydens, S. Geuens, M. Moremans, J. deMey, and P. Hollenbeck. 1987. Nanovid tracking: a new automatic method for the study of mobility in living cells based on colloidal gold and video microscopy. *Biophys. J.* 52:775–782.

Gelles, J., B. J. Schnapp, and M. P. Sheetz. 1988. Tracking kinesin-driven movements with nanometre-scale precision. *Nature.* 331:450–453.

Gennarini, G., M.-R. Hirch, H.-T. He, M. Hirn, J. Finne, and C. Goridis. 1986. Differential expression of mouse neural cell-adhesion molecule [N-CAM] mRNA species during brain development and in neural cell lines. *J. Neurosci.* 6:1983–1990.

Golan, D. E., and W. Veatch. 1980. Lateral mobility of band 3 in the human erythrocyte membrane studied by fluorescence photobleaching recovery: evidence for control by cytoskeletal interaction. *Proc. Natl. Acad. Sci. USA.* 77:2537–2541.

Gross, D. J., and W. W. Webb. 1988. Spectroscopic Membrane Probes, Vol. 1. CRC Press, Boca Raton, FL. 19–45.

Hicks, B. W., and K. Angelides. 1995. Tracking movements of lipids and Thy1 molecules in the plasmalemma of living fibroblasts by fluorescence video microscopy with nanometer scale precision. *J. Membr. Biol.* 144:231–244.

Jacobson, K., A. Ishihara, and R. Inman. 1987. Lateral diffusion of proteins in membranes. *Annu. Rev. Physiol.* 49:163–175.

Jacobson, K. A., S. E. Moore, B. Yang, P. Doherty, G. W. Gordon, and Walsh, F. S. 1997. Cellular determinants of the lateral mobility of neural cell adhesion molecules. *Biochim. Biophys. Acta.* 1330:138–144.

Jacobson, K., E. D. Sheets, and R. Simson. 1995. Revisiting the fluid mosaic model of membranes. *Science.* 268:1441–1442.

Jain, M. K., and H. B. White. 1977. Long range order in biomembranes. *Adv. Lipid Res.* 15:1–60.

Kemler, R. 1993. From caherins to catenins: cytoplasmic protein interactions and regulation of cell adhesion. *Trends Genet.* 9:317–321.

Kusumi, A., and Y. Sako. 1996. Cell surface organization by the membrane skeleton. *Curr. Opin. Cell Biol.* 8:566–574.

Kusumi, A., S. Yasushi, and M. Yamamoto. 1993. Confined lateral diffusion of membrane receptors as studied by single particle tracking (nanovid microscopy). Effects of calcium-induced differentiation in cultured epithelial cells. *Biophys. J.* 65:2021–2040.

Lee, G. M., A. Ishihara, and K. Jacobson. 1991. Direct observation of brownian motion of lipids in a membrane. *Proc. Natl. Acad. Sci. USA.* 88:6274–6278.

Lee, G. M., F. Zhang, A. Ishihara, C. L. McNeil, and K. A. Jacobson. 1993. Unconfined lateral diffusion and an estimate of pericellular matrix viscosity revealed by measuring the mobility of gold tagged lipids. *J. Cell Biol.* 120:25–35.

Moore, S. E., J. Thompson, V. Kirkness, J. G. Dickson, and F. S. Walsh. 1987. Skeletal muscle neural cell adhesion molecule (N-CAM): changes in protein and mRNA species during myogenesis of muscle cell lines. *J. Cell Biol.* 105:1377–1386.

Peck, D., and F. S. Walsh. 1993. Differential effects of over-expressed neural cell adhesion molecule isoforms on myoblast fusion. *J. Cell Biol.* 123:1587–1595.

Peters, R. 1988. Lateral mobility of proteins and lipids in the red cell membrane and the activation of adenylate cyclase by beta-adrenergic receptors. *FEBS Lett.* 234:1–7.

Peters, R., and R. J. Cherry. 1982. Lateral and rotational diffusion of bacteriorhodopsin in lipid bilayers: experimental test of the Saffman-Delbrück equations. *Proc. Natl. Acad. Sci. USA.* 79:4317–4321.

Pollerberg, G. E., M. Schachner, and J. Davoust. 1986. Differentiation state-dependent surface mobilities of two forms of the neural cell adhesion molecule. *Nature.* 324:462–465.

Quian, H., M. P. Sheetz, and E. L. Elson. 1991. Single particle tracking analysis of diffusion and flow in two dimensional systems. *Biophys. J.* 60:910–921.

Ranscht, B. 1994. Cadherins and catenins: interactions and functions in embryonic development. *Curr. Opin. Cell Biol.* 6:740–746.

Rodgers, W., and M. Glaser. 1993. Distributions of proteins and lipids in the erythrocyte membrane. *Biochemistry.* 32:12591–12598.

Saffman, P. G., and M. Delbruck. 1975. Brownian motion in biological membranes. *Proc. Natl. Acad. Sci. USA.* 72:3111–3113.

Sako, Y., and A. Kusumi. 1994. Compartmentalized structure of the plasma membrane for receptor movements as revealed by a nanometer-level motion analysis. *J. Cell Biol.* 125:1251–1264.

Sako, Y., and A. Kusumi. 1995. Barriers for lateral diffusion of transferrin receptor in the plasma membrane as characterized by receptor dragging by laser tweezers: fence versus tether. *J. Cell Biol.* 129:1559–1574.

Saxton, M. J. 1993. Lateral diffusion in an archipelago. *Biophys. J.* 64: 1766–1780.

Saxton, M. J. 1994. Anomalous diffusion due to obstacles: a Monte Carlo study. *Biophys. J.* 66:394–401.

Saxton, M. J., and K. Jacobson. 1997. Single particle tracking: applications to membrane dynamics. *Annu. Rev. Biophys. Biomol. Struct.* 26: 373–399.

Schnitzer, J. E., D. P. McIntosh, A. M. Dvorak, J. Liu, and P. Oh. 1995. Separation of caveolae from associated microdomains of GPI-anchored proteins. *Science.* 269:1435–1439.

Schroeder, R., E. London, and D. Brown. 1994. Interactions between saturated acyl chains confer detergent resistance on lipids and glycosylphosphatidylinositol (GPI)-anchored proteins: GPI-anchored proteins in liposomes and cells show similar behavior. *Proc. Natl. Acad. Sci. USA.* 91:12130–12134.

Sheets, E. D., R. Simson, and K. Jacobson. 1995. New insights into membrane dynamics from the analysis of cell surface interactions by physical methods. *Curr. Opin. Cell Biol.* 7:707–714.

Sheets, E. D., G. M. Lee, R. Simson, and K. Jacobson. 1997. Transient confinement of a glycosylphosphatidylinositol-anchored protein in the plasma membrane. *Biochemistry*. 34:12449–12459.

Sheetz, M. P. 1993. Glycoprotein motility and dynamic domains in fluid plasma membranes. *Annu. Rev. Biophys. Biomol. Struct.* 22:417–431.

Sheetz, M. P., M. Schindler, and D. E. Koppel. 1980. Lateral mobility of integral membrane proteins is increased in sperocytic erythrocytes. *Nature.* 285:510–512.

Simson, R., E. D. Sheets, and K. A. Jacobson. 1995. Detection of temporary lateral confinement of membrane proteins using single-particle tracking analysis. *Biophys. J.* 69:989–993.

Small, S. J., S. L. Haines, and R. Akeson. 1988. Polypeptide variation in an NCAM extracellular fold is developmentally regulated through alternative splicing. *Neuron.* 1:1007–1017.

Tsuji, A., and S-I. Ohnishi. 1986. Restriction of the lateral motion of band 3 in the erythrocyte membrane by the cytoskeletal network: dependence on spectrin association state. *Biochemistry.* 25:6133–6139.

Walsh, F. S., and P. Doherty. 1991. Structure and function of the gene for neural cell adhesion molecule. *Semin. Neurosci.* 3:271–284.

Walsh, F. S., J. Furness, S. E. Moore, S. Ashton, and P. Doherty. 1992. Use of the neural cell adhesion molecule VASE exon by neurons is asociated with a specific downregulation of neural cell adhesion molecule-dependent neurite outgrowth in developing cerebellum and hippocampus. *J. Neurochem.* 59:1959–1962.

Williams, E. J., J. Furness, F. S. Walsh, and P. Doherty. 1994. Activation of the FGF receptor underlies neurite outgrowth stimulated by L1, N-CAM and N-cadherin. *Neuron.* 13:583–594.

Yechiel, E., and M. Edidin. 1987. Micrometer-scale domains in fibroblast plasma membranes. *J. Cell Biol.* 105:755–760.

Zhang, F., B. Crise, B. Su, Y. Hou, J. K. Rose, A. Bothwell, and K. Jacobson. 1991. Lateral diffusion of membrane-spanning and glycosylphosphatidylinositol-linked proteins: toward establishing rules governing the lateral mobility of membrane proteins. *J. Cell Biol.* 115: 75–84.

Zhang, F., G. M. Lee, and K. Jacobson. 1993. Protein lateral mobility as a reflection of membrane microstructure. *Bioessays.* 15:579–588.